Paper: ASAT-15-108-AE

15th International Conference on
AEROSPACE SCIENCES & AVIATION TECHNOLOGY,
ASAT - 15 – May 28 - 30, 2013, Email: asat@mtc.edu.eg ,
Military Technical College, Kobry Elkobbah, Cairo, Egypt,
Tel: +(202) 24025292 –24036138, Fax: +(202) 22621908

Investigating the Design Parameters of a Diamond-Shaped Supersonic Airfoil

{M. H. F. El-Gohary, M. Y. M. Ahmed*}†

Abstract: The lifting surfaces of supersonic flying vehicles generally have sharp leading edges. The airfoil sections of such wings produce the desired lift and, more importantly, yield less drag compared with the conventional blunt airfoils commonly used with subsonic flying vehicles.

It is evident that, under given flight conditions, the aerodynamic characteristics of a supersonic airfoil namely, its aerodynamic coefficients are strongly dependent on its geometry. More interestingly, the variation in these coefficients is non-monotonic with the variation in the airfoil design.

In the present paper, a parametric study is conducted on a diamond-shaped airfoil of a 10% thickness-to-chord ratio. The objective is to investigate the impact of the airfoil design on its performance. A computer code is developed based on the exact shock-expansion theory to estimate the pressure distribution over the airfoil and, hence, its corresponding aerodynamic coefficients. It was found that, the aerodynamic coefficients of the airfoil are sensitive to its design. In addition, the designs for maximum lift and minimum drag coefficients are competing. A nearly-symmetric airfoil would yield a maximum aerodynamic efficiency.

Keywords: Missile aerodynamics, supersonic airfoil, parametric study.

1. Introduction

In the flying vehicles, the aerodynamic forces, especially lift, are mainly generated by the control surfaces which are, thus, also known as the lifting surfaces. The value of the generated forces at given flight conditions varies with the design of these surfaces. The key parameter in the design of the lifting surfaces is the design of their sections; the airfoils.

The common designs of supersonic airfoils include two major families namely, the circular arc airfoils and the general hexagonal airfoils. The former can have a sharp or a blunt trailing edge whereas the latter can have a variety of derived shapes, Fig. 1. In all designs, the supersonic airfoil can be symmetric or non-symmetric about its chord line.

In contrast to subsonic and transonic airfoils, the supersonic airfoils are characterized by a sharp leading edge. This key design feature is intended to generate a straight, attached shock wave ahead of the airfoil much weaker than the detached bow shock wave generated ahead of airfoils with blunt leading edges. Downstream of the leading edge, the flow over the airfoil subsequently expands as it passes through a series of expansion waves. The typical flow pattern around a symmetric diamond-shaped airfoil at zero incidence is illustrated in Fig. 2.

* mym141101@yahoo.com ;
† Egyptian Armed Forces, Egypt.

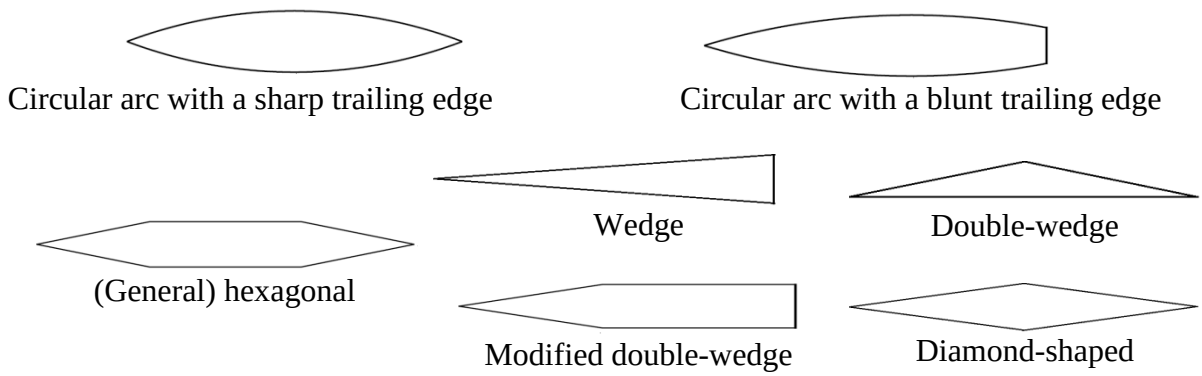

Figure 1. Typical shapes of supersonic airfoils

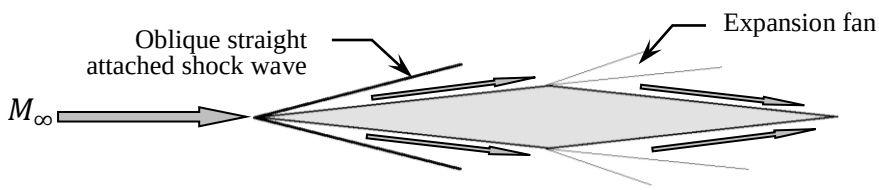

Figure 2. A typical flow pattern around a symmetric diamond-shaped airfoil at zero incidence

The flow pattern becomes more sophisticated as the complexity of the airfoil design increases, in cases of non-symmetric airfoils and/or at incidence. In all cases, the local flow direction is parallel to the airfoil surface whereas the local flow properties depend on the strengths of the shock waves and expansion fans. As a consequence, at given freestream Mach number, M_∞, and incidence angle, the aerodynamic coefficients of the airfoil are solely dictated by its design.

In the literature, there is a considerable body of studies that are devoted to investigating the aspects of supersonic airfoils design and their aerodynamic characteristics. In his experimental study, Alexander [1] briefly investigated the variation of the drag coefficient of a circular arc airfoil at different freestream velocities by analyzing a set of flight tests. Underwood and Nuber [2] measured the aerodynamic characteristics of circular arc airfoils. They also investigated the effect of adding high-lift devices to the plain airfoil at different incidence angles. The impact of adding leading- and trailing-edge flaps to symmetric diamond and circular arc airfoils on their aerodynamic coefficients was investigated theoretically by Morrissette and Oborny [3]. The pressure distribution over a circular arc airfoil at different incidence angles was measured by Boyd et. al [4]. They compared their experimental findings with the theoretical predictions. Vincenti [5] compared the experimental and theoretical aerodynamic coefficients of circular arc and diamond airfoils. He also investigated the impact of the shape of the diamond airfoil on its characteristics. Ulmann and Lord [6] studied experimentally the impact of the thickness of the circular arc airfoil on the pressure distribution over it at different freestream conditions.

In his comprehensive study, Chapman [7] conducted a series of experiments on supersonic airfoils with various shapes. He investigated the impact of freestream conditions, incidence angle, airfoil shapes, on the airfoil base drag. The study was extended by Goin [8]. He investigated the impact of the design of blunt-trailing edge airfoils on the base pressure of a winged slender body at low supersonic conditions. The analytical study of Eggers et. al [9]

focused on the circular arc airfoil. They compared a variety of analytical methods in predicting the aerodynamics characteristics and the flowfield pattern around the airfoil at different freestream velocities and incidences. Chapman [10] conducted another comprehensive theoretical investigation to find the profile of a blunt trailing-edge circular arc airfoil that provides minimum drag at zero incidence. Katzen et al. [11] conducted a comprehensive experimental study on circular arc airfoils with both pointed and blunt trailing edges. The impact of the airfoil design on its aerodynamic coefficients at different freestream conditions was thoroughly investigated.

While the above studies used theoretical and experimental approaches, the more recent studies of supersonic airfoils implemented the numerical CFD techniques. Dutt and Sreekanth [12], conducted an area-constrained, drag minimization study for a symmetric circular arc airfoil at zero incidence. The drag coefficient was calculated based on an analytical one-dimensional equation for the pressure distribution over the airfoil. Pittman [13] conducted a design optimization for a supersonic wing with a cambered circular arc airfoil. The optimization problem was intended to minimize the drag subject to a minimum lift constraint. Tai and Moran [14] investigated numerically the flow over a symmetric circular arc airfoil along with some NACA symmetric subsonic airfoils. Their focus was to study the supersonic low-density flow resembling the high-altitude high-speed flight conditions. Their findings included the lift, drag coefficients, and pressure coefficient distribution over such airfoils. Finally, the recent study of Hu et al. [15] focused on finding the optimum design of a double-wedge biplane airfoil for minimum drag at zero incidence.

It is clear that, almost all the previous studies focused on the circular arc airfoils with both sharp and blunt trailing edges. The hexagonal airfoils have gained significantly less attention by the researchers. A study of the design parameters of hexagonal airfoils could not be found in the open literature. Moreover, the aspects of non-symmetric airfoils was not thoroughly investigated so far.

The shock-expansion theory [16] is an exact theory that is derived from the fundamental governing equations of inviscid compressible flow. It is based on a stepwise treatment of the supersonic flow over a body of arbitrary shape as a set of shock waves and expansion fans. By treating each of them separately, the flow properties over the entire body, such as the airfoil in Fig. 2, can be estimated for known freestream flow properties. Vincenti [5] showed that the results from the shock-expansion method are in excellent agreement with the experimental measurements. Eggers et al. [9] confirmed the accuracy of this method even for high Mach numbers as long as the oblique shock waves remain attached.

In the present paper, a parametric study of non-symmetric diamond-shaped airfoils is conducted. The objective of the study is to understand the role of airfoil shape in deciding its aerodynamic characteristics namely lift, drag, moment coefficients, and centre of pressure at different freestream Mach numbers and incidence angles. These calculation of the aerodynamic characteristics is based on the results of the shock-expansion theory. The reminder of the paper is organized as follows. The test case and the study methodology are presented in the next section. The main results are illustrated and discussed later and the paper finalizes with highlighting the main conclusions along with recommendations for further investigations.

2. Case Study and Methodology

2.1. The Case Study

A non-symmetric diamond-shaped airfoil of a unit chord, $c = 1$, representing the section of a unit-span wing, is considered. The maximum thickness of both the upper and lower surfaces are fixed and equal to 5% of the chord whereas the locations of the maximum thickness per chord on both surfaces, l_u and l_l, are variable and different, Fig. 3.

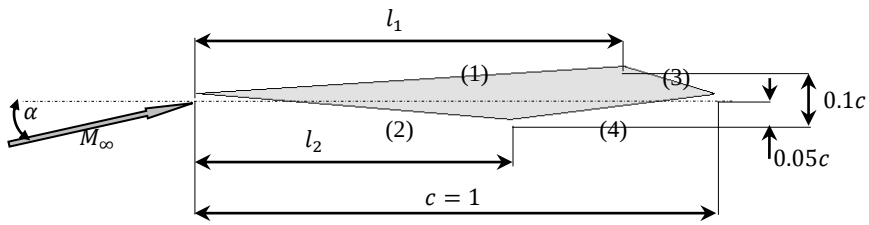

Figure 3. Geometry of the test case

The airfoil is exposed to a supersonic freestream of Mach, $M_\infty > 1$, at an incidence angle, $\alpha > 0$. At given values of M_∞ and α, surface (1) can have a shock wave or an expansion fan depending on the value of l_1. In contrast, regardless to the freestream conditions, surface (2) always experiences a shock wave for all values of l_2 while an expansion fan is always developed on both surfaces (3) and (4). The minimum values of l_1 and l_2 should be such that an attached shock wave is guaranteed on surfaces (1) and (2), respectively.

2.2 Methodology

By varying the values of l_1 and l_2, different designs can be attained. Consequently, the design space in concern is two-dimensional with l_1 and l_2 as the coordinates. They are varied independently from their corresponding minimum values up to c with 50 intermediate steps. A full factorial sampling is adopted thus generating 2500 distinct designs from the entire design space.

The results of the shock-expansion theory are used to calculate the pressure distribution over the four surfaces of all airfoil designs, $c_{p_i}, i \in [1,4]$. Once calculated, the aerodynamic characteristics of each design namely, the lift coefficient, drag coefficient, pitching moment coefficient about the leading edge, aerodynamic efficiency, and the center of pressure, are evaluated according to the following relations:

The normal force coefficient:

$$c_n = c_{p_2} l_2 + c_{p_4}(1 - l_2) - c_{p_1} l_1 - c_{p_3}(1 - l_1) \tag{1}$$

The axial force coefficient:

$$c_a = 0.05\left[c_{p_1} l_1 + c_{p_2} l_2 - c_{p_3}(1 - l_1) - c_{p_4}(1 - l_2)\right] \tag{2}$$

The moment coefficient:

$$c_m = -0.5\left[c_{p_2} {l_2}^2 + c_{p_4}(1 - l_2)(1 + l_2) - c_{p_1} {l_1}^2 - c_{p_3}(1 + l_1)\right] \tag{3}$$

The center of pressure:

$$\bar{x}_{cp} = x_{cp}/c = c_m/c_l \tag{4}$$

The lift coefficient:

$$c_l = c_n cos\alpha - c_a sin\alpha \tag{5}$$

The drag coefficient:

$$c_d = c_n sin\alpha + c_a cos\alpha \tag{6}$$

The aerodynamic efficiency:

$$\eta = c_l / c_d \tag{7}$$

In the above relations, the reference area and length are the $(chord \times span)$ and $(chord)$, respectively, both having the value of one. A computer code written in C++ language is developed to automate the calculations. The code also calculates all local flow properties such as Mach number, temperature and density ratios (relative to their freestream counterparts) over the entire airfoil. To validate the code, one case from the work of Ivey et al. [16] is investigated using the developed code. The validation case is a symmetric diamond-shaped airfoil of equal leading and trailing-edge angles of 2° placed at 3° incidence in a Mach 4 freestream. Table 1 holds a comparison between the reported and calculated values of local pressure coefficients and Mach numbers on the four surfaces of the airfoil. The accuracy of calculations of the code is assumed acceptable.

Table 1 Validation results for the calculation code

	Local pressure coefficient		Local Mach number	
	Ivey et al. [16]	Code	Ivey et al. [16]	Code
Forward windward	0.0416	0.042	3.7	3.71
Rearward windward	0.0188	0.019	3.84	3.86
Forward leeward	-0.0169	-0.0163	4.16	4.156
Rearward leeward	-0.0308	-0.0306	4.33	4.32

3. Results and Discussions

The impact of the airfoil design on its aerodynamic characteristics is investigated at freestream Mach number and incidence angle of 2 and 5°, respectively.

Lift Coefficient

The carpet curve below, Fig. 4, shows the variation of the lift coefficient in the entire design space.

It can be also inferred that the roles of l_1 and l_2 in deciding the lift are competing in some sense. To understand this more clearly, the variation of c_l with l_1 at a given l_2 and the variation of c_l with l_2 at a given l_1 are illustrated in Fig. 5a and b, respectively.

In addition, by comparing Fig. 5.a and b, It can be shown that the minimum length for surface (1) is smaller than that of surface (2). This may be explained by the fact that the shock wave acting on the latter is stronger than that on the former which implies a smaller maximum deflection and, hence, a longer minimum length of surface (2). More importantly, by increasing l_1 for a given value of l_2, the lift increases, reaches some maximum value, and then decreases. To understand this phenomenon more clearly, the variation of the local pressure coefficients on the upper surfaces, c_{p_1} and c_{p_3}, and their area-weighted sum,

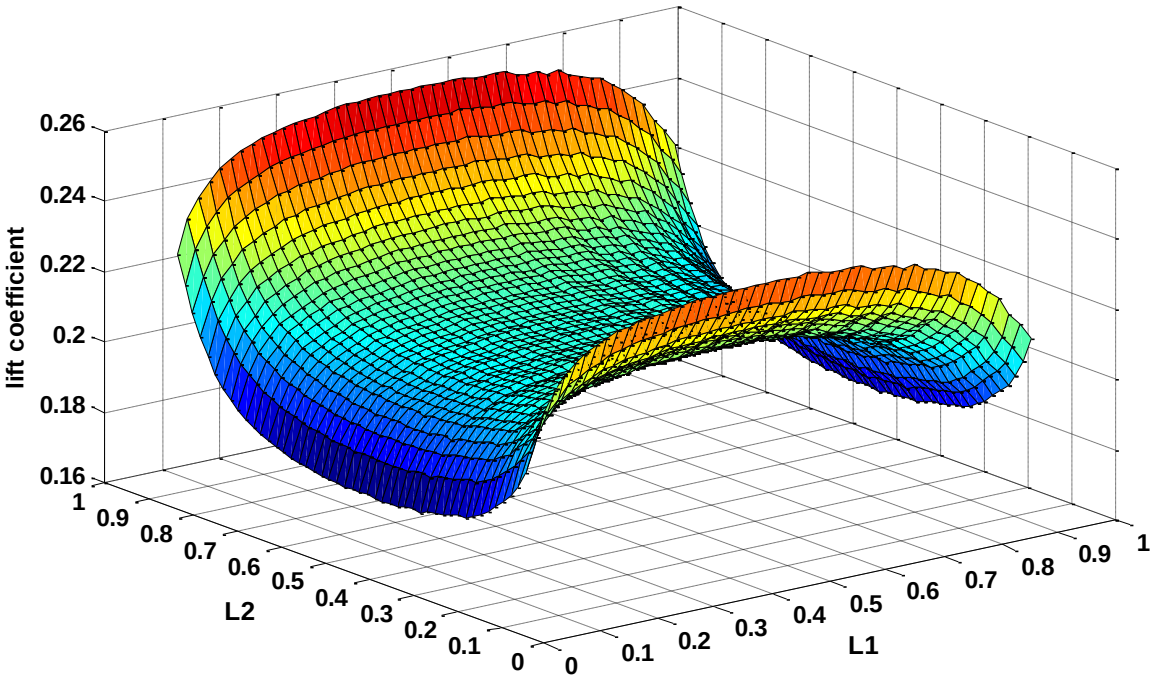

Figure 4. Impact of the airfoil design on the lift coefficient

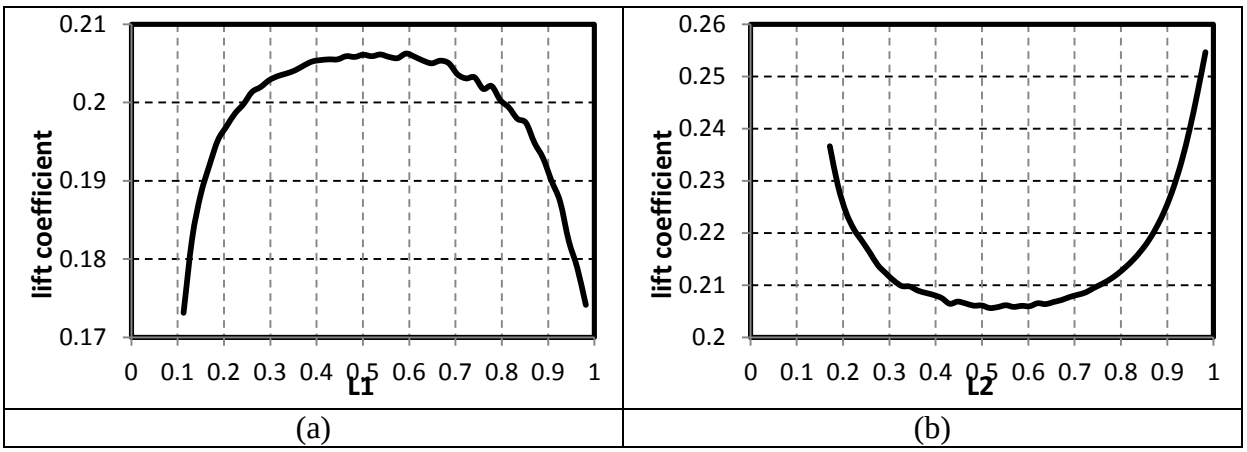

Figure 5. Variation of c_l with (a) l_1 at a given l_2, and (b) l_2 at a given l_1

$$c_{p_u} = c_{p_1} l_1 + c_{p_3}(1 - l_1),$$

with l_1 at a given l_2 is illustrated in Fig. 6 below.

At very small values of l_1, the local pressure coefficient on surface (1) attains high positive values due to the strong shock wave at the leading edge. Despite that, the strong subsequent expansion ahead of surface (3) yields a negative pressure coefficient over the latter. As l_1 slightly increases, both the flow compression angle ahead of surface (1) and expansion angle ahead of surface (3) decrease. This is illustrated in Fig. 7a below. As a consequence, the strengths of both the shock wave and the expansion fan decrease with l_1. However, it can be inferred that the drop in the strength of the shock wave is significantly more pronounced than the drop in the strength of the expansion fan.

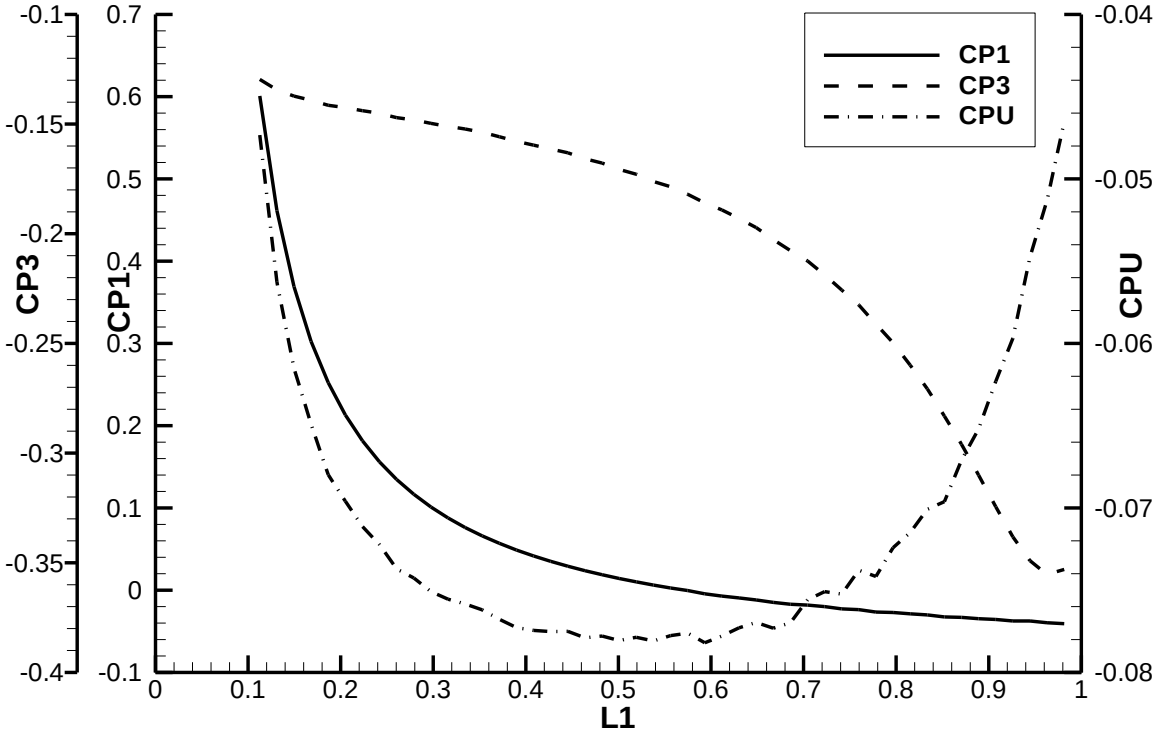

Figure 6. Variation of the local pressure coefficients on the upper surfaces (1) and (3) and their area-weighted sum with l_1

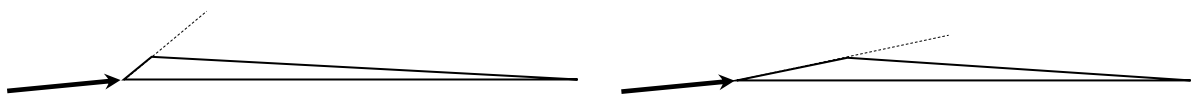

(a) As l_1 increases, the flow deflection angles on the upper surface decrease

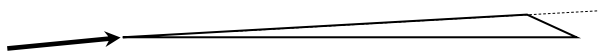

(b) As l_1 increases above 0.5, the flow expansion angle ahead of surface (3) increases again

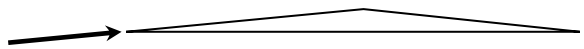

(c) At a specific value of l_1, the incoming flow experiences no deflection on surface (1)

Figure 7. Variation of the flow attitude over the upper surfaces with l_1

As the geometry implies, the expansion angle ahead of surface (3) and, consequently, the strength of the expansion fan over it decrease as l_1 increases below 0.5 and increase again as l_1 increases beyond 0.5, Fig. 7b. On the other hand, the strength of the shock wave at the leading edge decreases monotonically as l_1 increases until the latter reaches a specific value at which the incoming flow experiences no deflection at all on surface (1), Fig. 7c.

It is also interesting to note that both c_{p_3} and c_{p_u} always have negative values even with highly positive values of c_{p_1}. This can be explained recalling that such values of c_{p_1} are associated with an expansion ahead of surface (3) strong enough to reduce c_{p_3} below zero. Both c_{p_1} and the strength of the expansion fan decrease as l_1 increases such that c_{p_3} remains negative. In addition, the high positive values of c_{p_1} are associated with small areas of surface (1) while the corresponding negative values of c_{p_3} are associated with large areas of surface (3). The overall effect of the local pressure coefficients and the areas is that c_{p_u} becomes negative for all values of l_1. Likewise, the overall effect these two factors may explain the rise in c_{p_u} as l_1 approaches 1. Since lift is composed primarily from the projection of the pressure distribution in the normal direction, the trend of c_l with l_1 is identical to that of c_{p_u} with l_1.

In contrast, for a given l_1, lift decreases with increasing l_2, reaches some minimum value, and then increases again, Fig. 5b. The rates of lift drop and rise with l_2 are almost similar. To understand this phenomenon more clearly, the variation of the local pressure coefficients on the lower surfaces, c_{p_2} and c_{p_4}, and their area-weighted sum, $c_{p_l} = c_{p_2} l_2 + c_{p_4}(1 - l_2)$, with l_2 at a given l_1 is illustrated in Fig. 8 below.

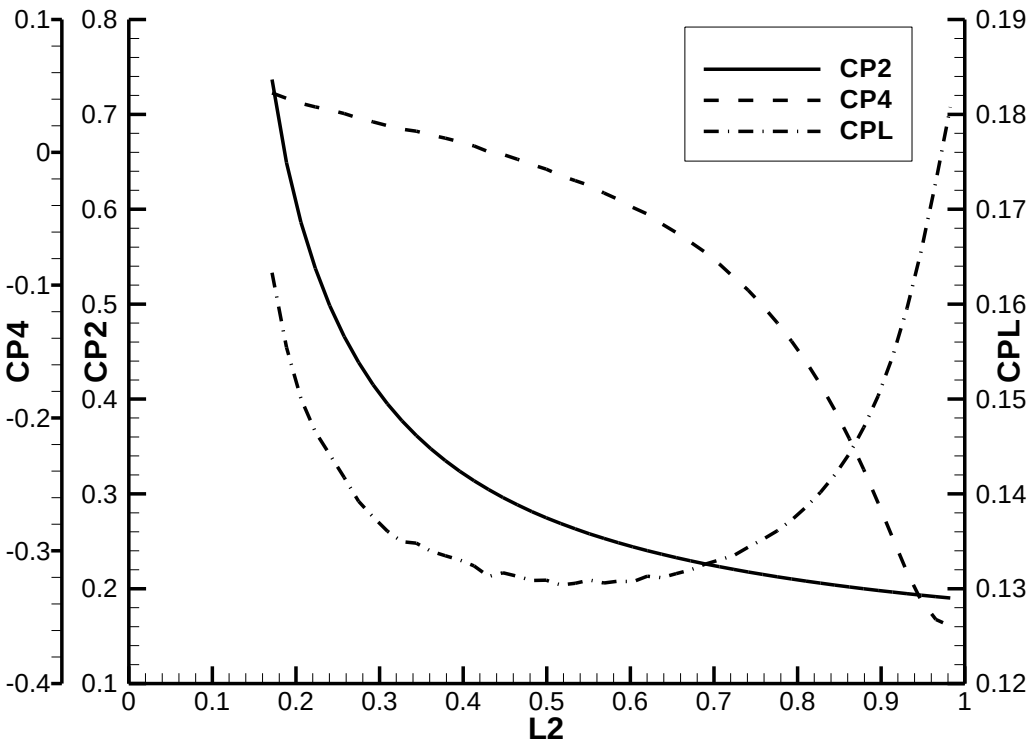

Figure 8. Variation of the local pressure coefficients on the lower surfaces (2) and (4) and their area-weighted sum with l_2

At very small values of l_2, the strength of the oblique shock wave generated ahead of surface (2) is maximum yielding very high values of c_{p_2}. The subsequent expansion ahead of surface (4) has the role of reducing the pressure over surface (4) significantly, however, it is not

strong enough to bring c_{p_4} below zero. As l_2 increases, the strength of the forward shock wave decreases, causing both c_{p_2} and c_{p_4} to decrease with the latter becoming negative. The shock wave is always present ahead of surface (1) and thus, c_{p_2} remains positive for all values of l_2. In addition, as l_2 increases, the area exposed to c_{p_2} increases while the area exposed to c_{p_4} decreases. The overall effects of the pressure coefficients and the associated areas yield the trend of c_{p_l} shown in Fig. 8. Similarly, the trend of c_l with l_2 is identical to that of c_{p_l} with l_2.

It is also interesting to investigate the designs that produce extreme lift merits. The airfoil designs that yield maximum and minimum lift coefficients are compared in Table 2. The drawn airfoil designs are such that the incoming flow direction is rightwards.

Table 2. Comparison between airfoil designs with extreme lift coefficients

	Value	Design	l_1	l_2
Maximum lift coefficient	0.2548		0.59	0.98
Minimum lift coefficient	0.1726		0.11	0.52

It is worth addressing here that 0.11 and 0.98 are, respectively, the minimum value of l_1 and the maximum value of l_2 for all the designs investigated. It can thus be inferred the maximum lift is associated with a maximum l_2 whereas the minimum lift is associated with l_1. Despite that smaller values of l_2 would yield higher c_{p_2} (which would mean higher lift), the role of the associated smaller areas of surface (2) may yield lower lift. Similarly, higher values of $l_1$yield lower c_{p_1}(which would mean lower lift), however, the role of the associated larger areas of surface (1) may yield higher lift. In fact, the impact of l_1 and l_2 is twofold; they dictate the values of the local pressure coefficients and they also dictate the associated areas which these pressure coefficients affect.

Drag Coefficient

The carpet curve in Fig. 9 below illustrates the variation of the drag coefficient with the design of the airfoil on the entire design space.

In contrast to c_l, the roles of l_1 and l_2 in deciding the drag coefficient are somehow similar. c_d decreases with the increase of l_1 and l_2, it reaches a minimum value halfway along l_2 and increases again. The rise in c_d at high l_1 is minor compared with that with l_2. This is illustrated more clearly in Fig. 10 below.

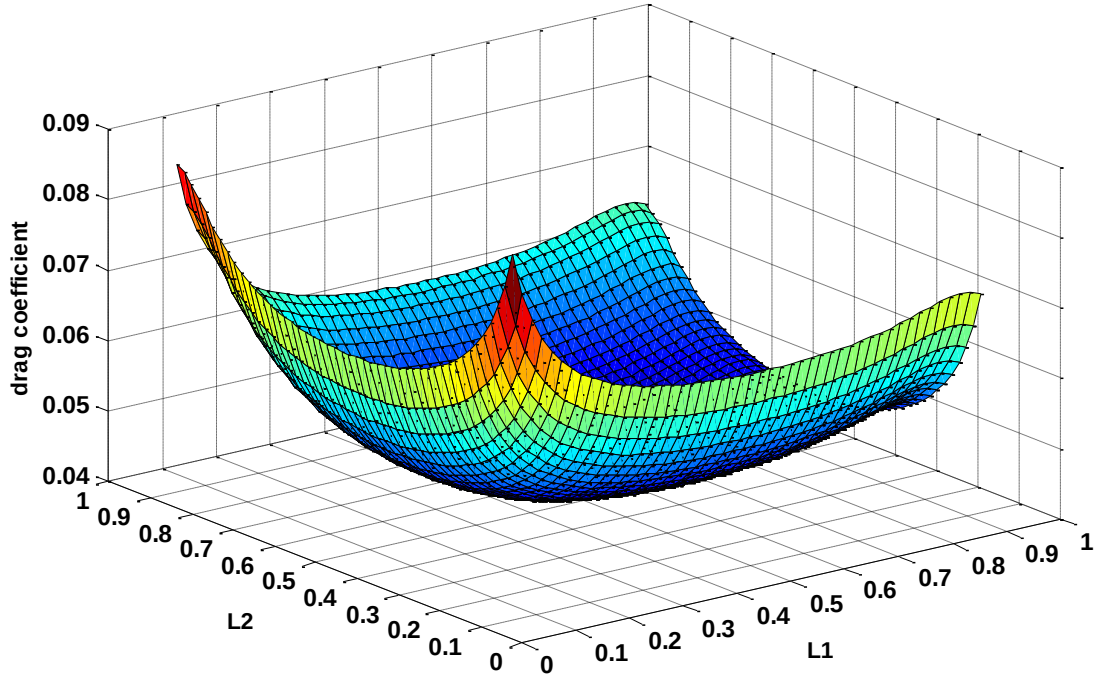

Figure 9. Impact of the airfoil design on the drag coefficient

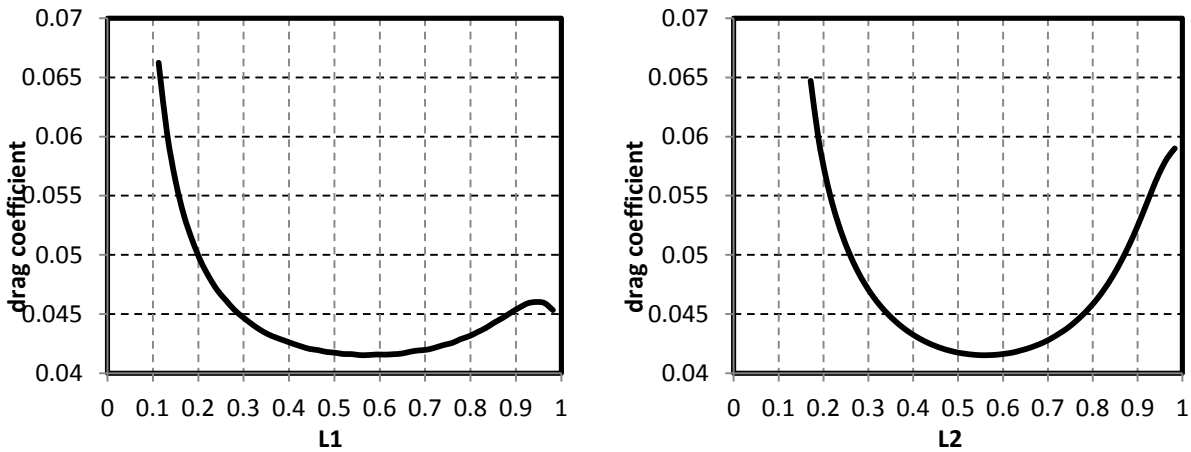

(a) (b)

Figure 10. Variation of c_d with (a) l_1 at a given l_2, and (b) l_2 at a given l_1

The trend of the drag coefficient can be explained recalling that the drag is primarily composed of the projection of the surface pressures on all surfaces of the airfoil in the axial direction. Figure 11 below illustrates the variation of the net upper and lower surfaces pressures in the axial direction.

The forward surfaces (1) and (2) always have higher pressures than the rearward ones (3) and (4). The trend and values of the drag coefficient depend on the mutual differences dictated by the values of l_1 and l_2. The airfoil designs that yield maximum and minimum drag coefficients are compared in Table 3. The drawn airfoil designs are such that the incoming flow direction is rightwards.

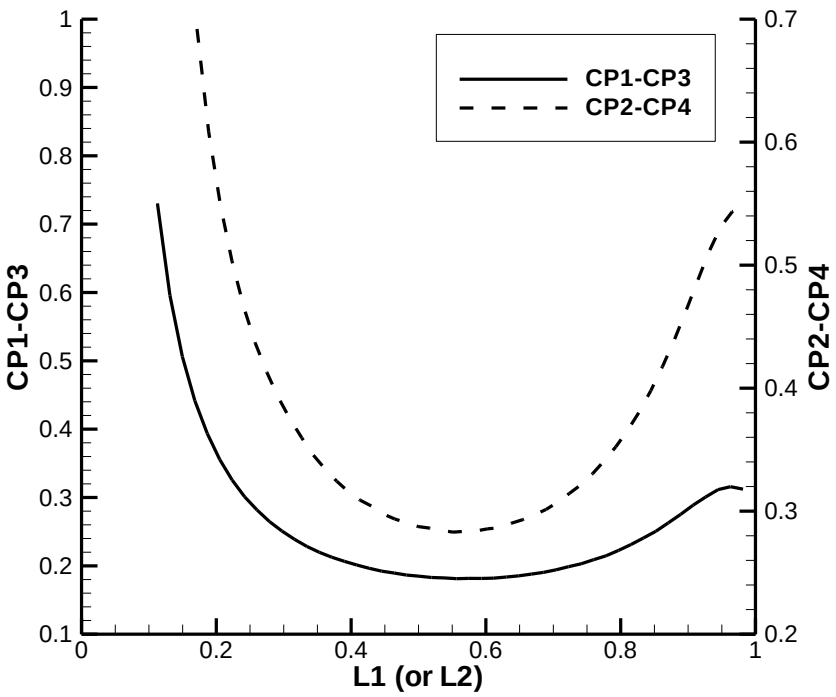

Figure 11. Variation of the net surface pressure on the upper and lower surfaces with the airfoil design

Table 3. Comparison between airfoil designs with extreme drag coefficients

	Value	Design	l_1	l_2
Minimum drag coefficient	0.0398		0.56	0.55
Maximum drag coefficient	0.089	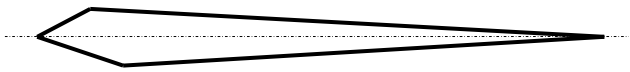	0.11	0.17

The design that produces a maximum drag possesses the shortest forward surfaces possible. This can be explained recalling that the associated values of the local pressure coefficients on the forward surfaces are maximum. Moreover, the value of l_1 associated with minimum drag is the switching value explained earlier. It can be easily shown that this value yields the minimum positive value of c_{p_1} which results in minimizing the drag.

Comparing the trends of lift and drag coefficients over the design space, Fig. 4 and 9, and the designs that yield extreme performance, Table 1 and 2, indicate that both performance merits may be competing. A single design that satisfies both high lift and low drag may not be attained. This invokes the need to investigate the aerodynamic efficiency, c_l/c_d, of the airfoils in concern.

Aerodynamic efficiency:

The carpet curve shown in Fig. 12 illustrates the variation of the aerodynamic efficiency over the entire design space.

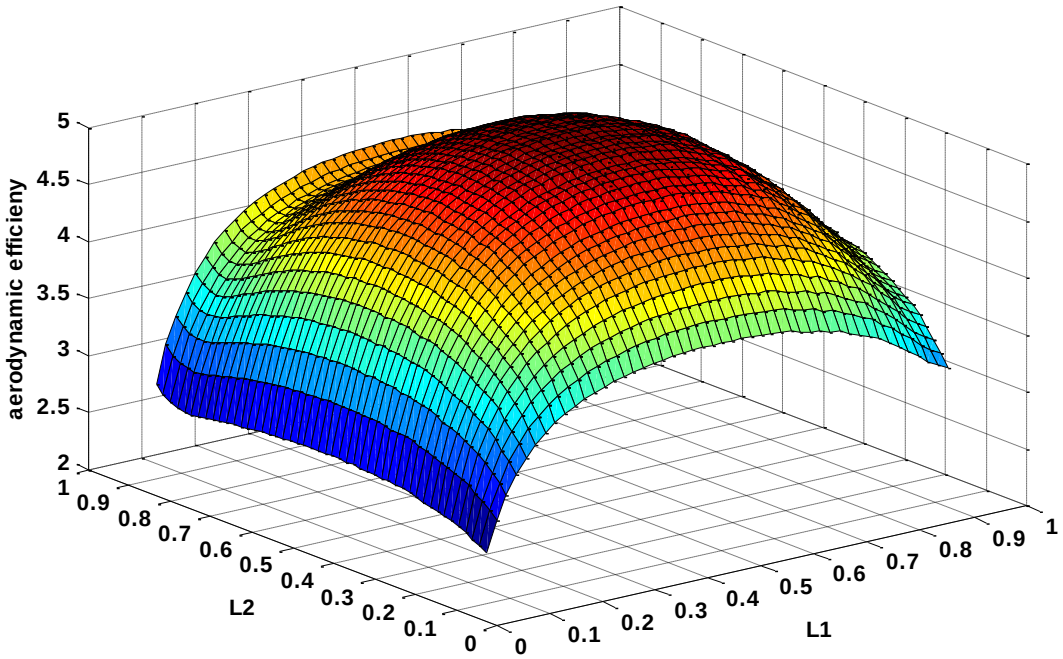

Figure 12. Impact of the airfoil design on its aerodynamic efficiency

It is clear that the trend of variation of the aerodynamic efficiency with l_1 and l_2 is the same; it is low for extreme values and high for intermediate values of the design parameters. It is interesting to note that the aerodynamic efficiency becomes maximum nearly in the middle of the design space. The airfoil designs that yield maximum and minimum aerodynamic efficiency are compared in Table 4. The drawn airfoil designs are such that the incoming flow direction is rightwards.

Table 4. Comparison between airfoil designs with extreme aerodynamic efficiency

	Value	Design	l_1	l_2
Maximum aerodynamic efficiency	4.98		0.59	0.55
Minimum aerodynamic efficiency	2.28	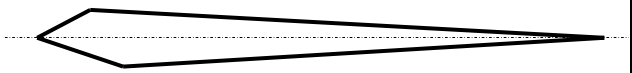	0.11	0.17

The design that possesses the minimum aerodynamic efficiency is the one that produces the maximum drag. More interestingly, the design with the maximum aerodynamic efficiency is almost symmetrical.

Pitching moment coefficient:

The carpet curve shown in Fig. 13 illustrates the attitude of the coefficient of the pitching moment about the leading edge over the entire design space. The variations of the pitching moment coefficient with l_1 and a given l_2 and with l_2 at a given l_1 are illustrated in Fig. 14.a and b, respectively.

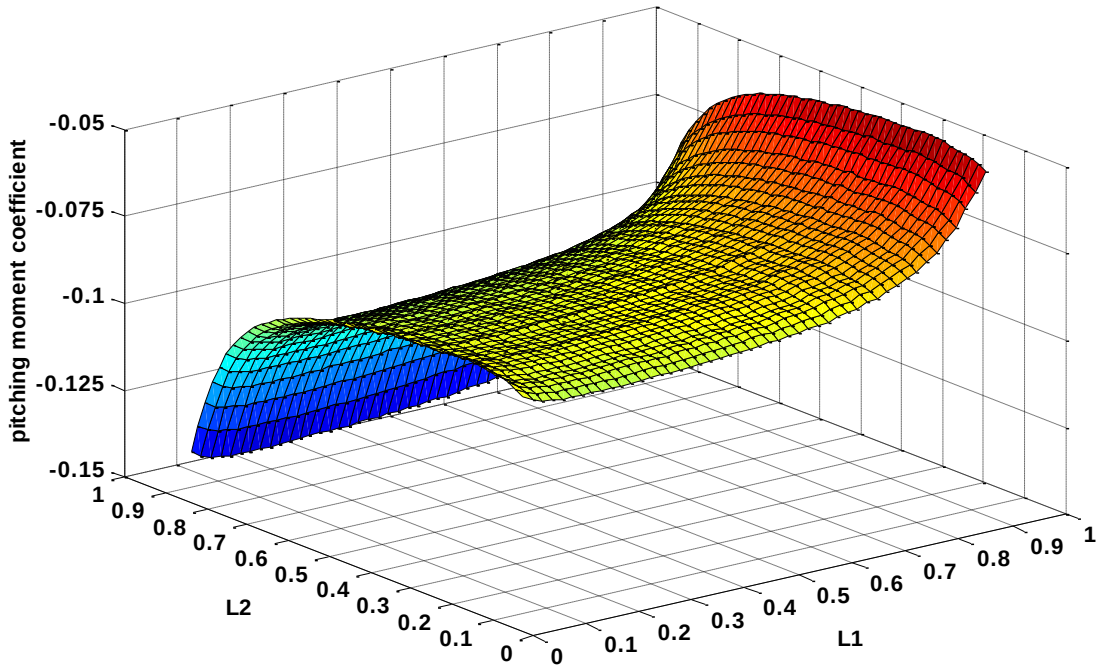

Figure 13. Impact of the airfoil design on its pitching moment

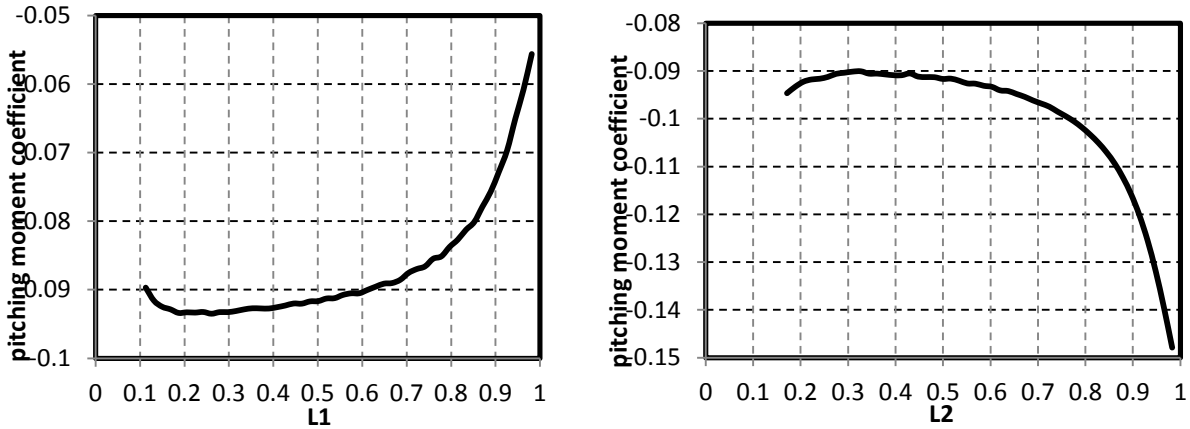

(a) (b)

Figure 14. Variation of c_m with (a) l_1 at a given l_2, and (b) l_2 at a given l_1

While the negative sign of c_m reflects its direction, its absolute value reflects its magnitude. In general, the magnitude of c_m decreases as l_1 increases. The slope of c_m drop increases at high values of l_1 and for very small values of l_1, c_m increases rather than decreases. In contrast, the magnitude of c_m increases as l_2 increases. The slope of c_m rise increases at high values of l_2 and for very small values of l_2, c_m decreases rather than increases. These phenomena can be understood recalling the combined effect of the local pressure coefficients and the associated areas. In fact, the impact of l_1 and l_2 on c_m is threefold; they govern the values of the local pressure coefficients, their associated areas, and the distance to the airfoil's leading edge. For instance, as l_1 increases, the local pressure coefficient decreases, the area of surface (1) increases, and the arm of the resultant pressure force to the leading edge increases. The combined effect of these three factors eventually dictate the value of the pitching moment. The airfoil designs that yield maximum and minimum pitching moment coefficients are

compared in Table 5. The drawn airfoil designs are such that the incoming flow direction is rightwards.

Location of the center of pressure:

The carpet curve shown in Fig. 15 illustrates the variation of the center of pressure location over the entire design space.

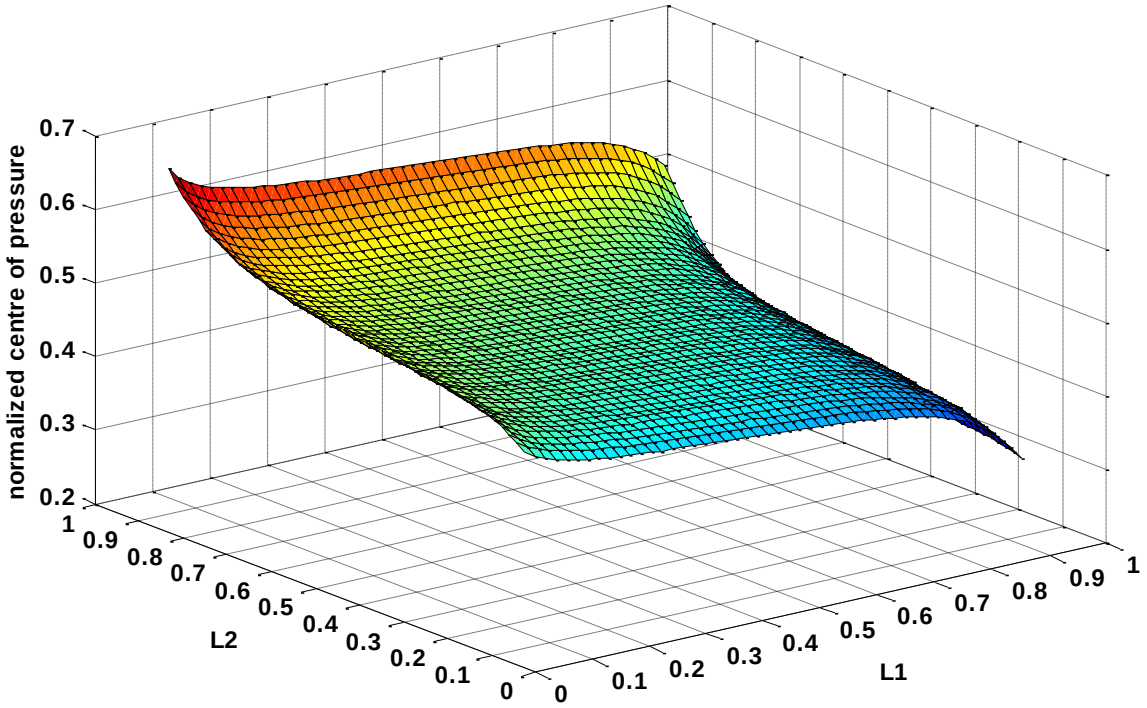

Figure 15. Impact of the airfoil design on the location of its center of pressure

The center of pressure shifts towards the airfoil leading edge as l_1 increases. In contrast, increasing l_2 has the role of shifting the centre of pressure towards the airfoil trailing edge. As in the case of the pitching moment coefficient, the impact of l_1 and l_2 on the centre of pressure location is complicated due to the variation of pressure distribution over the airfoil surfaces, the associated areas, and the distances to the leading edge. The airfoil designs that yield maximum and minimum pitching moment coefficients are compared in Table 6. The drawn airfoil designs are such that the incoming flow direction is rightwards.

Table 5. Comparison between airfoil designs with extreme pitching moment coefficient

	Value	Design	l_1	l_2
Maximum pitching moment coefficient	-0.1497		0.26	0.98
Minimum pitching moment coefficient	-0.054	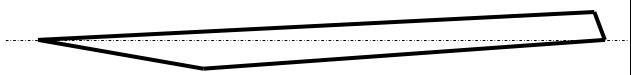	0.98	0.33

Table 6. Comparison between airfoil designs with extreme center of pressure locations

	Value	Design	l_1	l_2
Maximum location	0.64	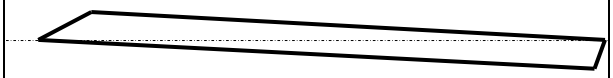	0.094	0.983
Minimum location	0.28	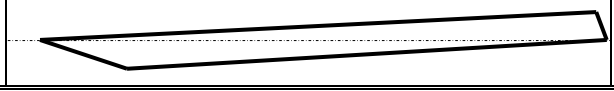	0.9815	0.1541

It is interesting to find out that the values of l_1 and l_2 are also the extremes. The centre of pressure becomes closest to the trailing edge if l_1 is minimum and l_2 is maximum; it becomes closest to the leading edge if l_1 is maximum and l_2 is minimum.

It also useful to explore the details of the flowfield around the form of the airfoils in concern. This can be exclusively done by making use of computational fluid dynamics (CFD) techniques. Due to the large number of designs investigated, a sample design is selected for this purpose. The airfoil that produces the maximum aerodynamic efficiency is taken as the single case study a commercial CFD code [17] is used. A multi-block structured two-dimensional grid is constructed around the airfoil. The form of the discretized computational domain and the definiton of the flow inlet and exit boundaries are illustrated in Fig. 16a. The grid is designed to be clustered over the airfoil surfaces and at their intersections. Zoom-ins at the airfoil leading edge are illustrated in Fig. 16b and c.

The steady, inviscid, density-based solver is used for simlating the flow around the airfoil. Upon convergence of the numerical solution, the numerical flowfield features can be displayed. Figure 17 a and b show the Mach and pressure contours around the airfoil, respectively.

Cleraly, a shock wave is generated ahead of surface (2) as indicated by the sudden change in the contours color. The flow expands ahead of surfaces (3) and (4) as indicated by the gradual change in the contours color. It is also interesting to note that the flow experiences neither expansion nor compression ahead of surface (1) since the deflection angle of this surface is 4.85^o which is very close to the value of the incidence angle. The value of the aerodynamic efficiency as calculated by the CFD solver is 4.975 which agrees very closely with that calculated using the shock-expansion theory, 4.9 (Table 4).

Conclusions

In this paper, a parametric study of diamond-shaped supersonic airfoil design has been conducted based on the results of the shock-expansion theory. It has been shown that the aerodynamic attitude of the airfoil in terms of the aerodynamic characteristics is strongly dependent on its design. More interestingly, these aerodynamic characteristics for a given design have shown a high degree of competition; simultaneously satisfying various characteristics may be unattainable. This may invoke the need for a multi-objective design optimization of the airfoil which can be the topic of future studies. Further studies may involve different airfoil designs such as modified diamond-shaped or hexagonal airfoils. It should be noted that the results presented in this paper are limited to the potential flow assumption. Future studies should make use of CFD techniques to solve the flow around the airfoil more accurately taking the flow viscosity into account.

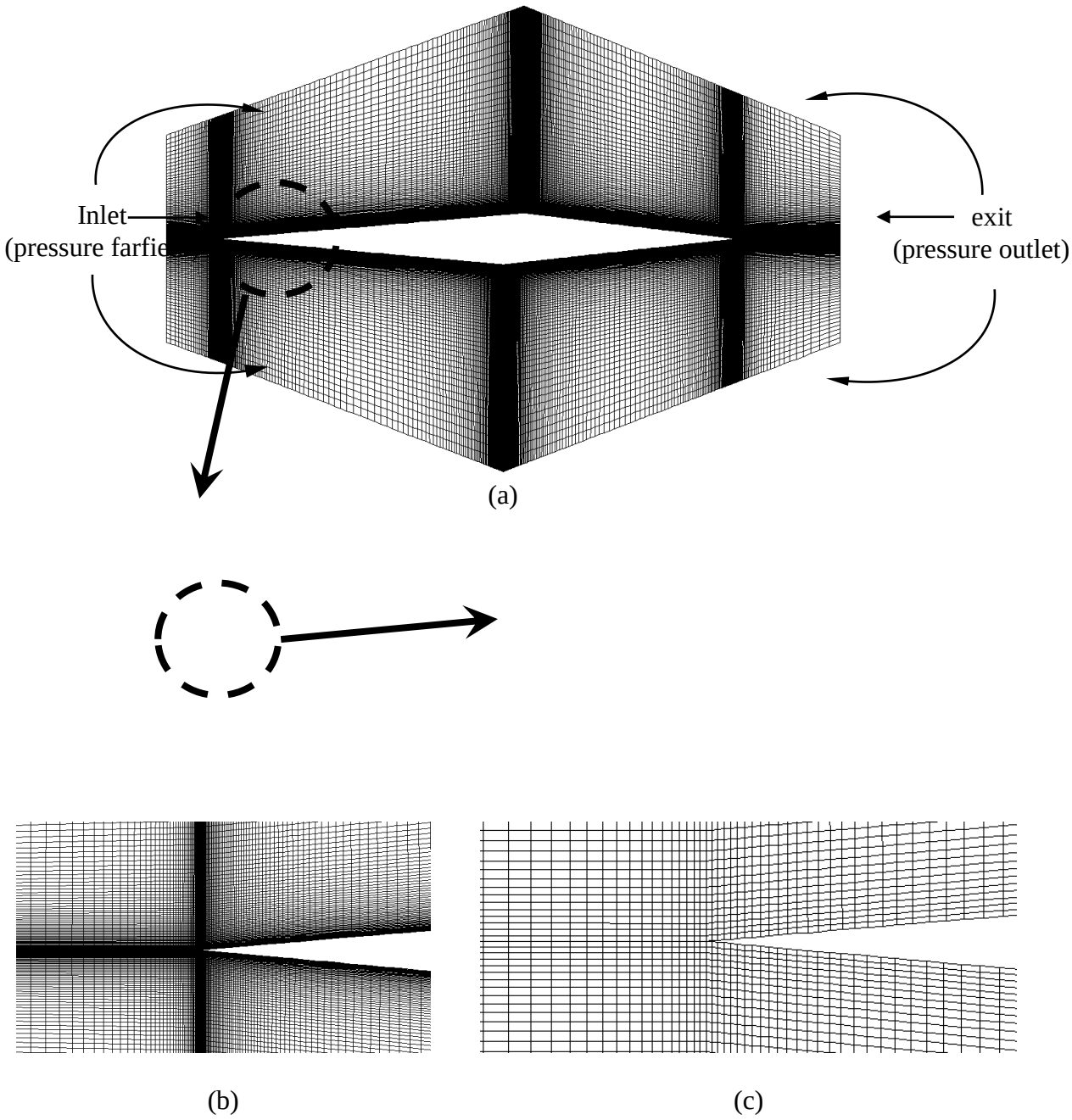

Figure 16 The computational domain around the airfoil

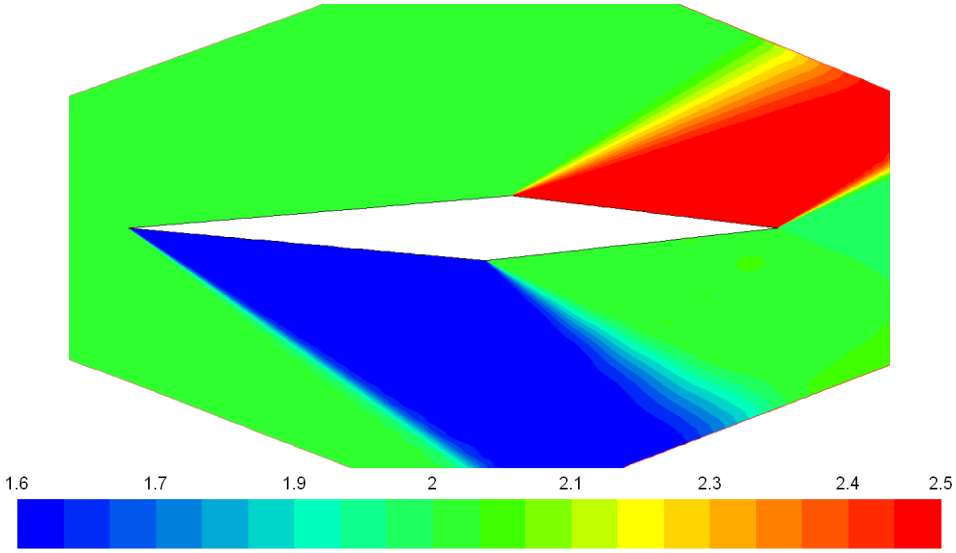

(a) Mach number contours

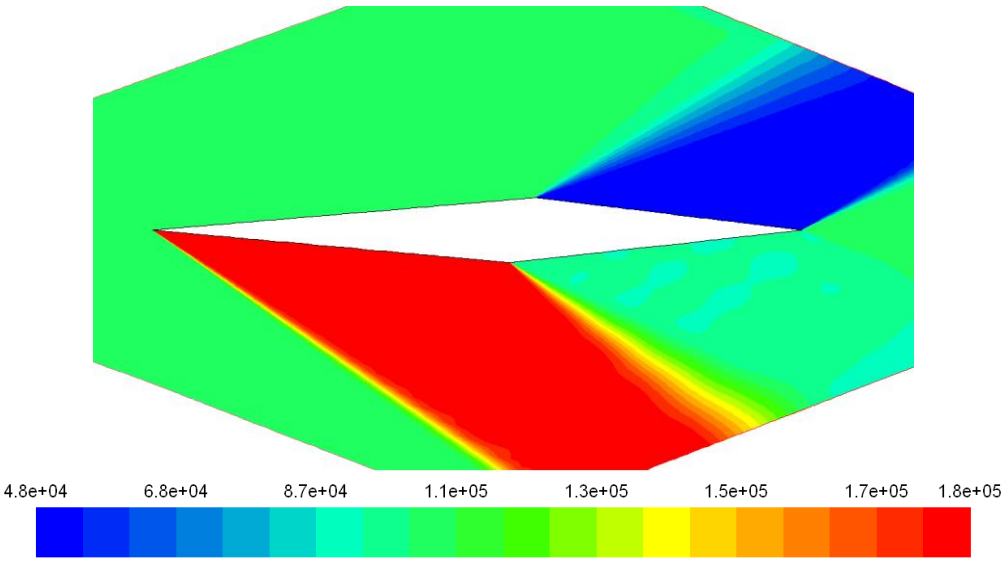

(b) Pressure contours

Figure 17 Features of the numerical flowfield around the airfoil with the maximum aerodynamic efficiency

References

[1] Alexander, S. R., "Drag Measurements of Symmetrical Circular-arc and NACA 65-009 Rectangular Airfoils Having an Aspect Ratio of 207 as Determined by Flight Tests at Supersonic Speed," NACA RM L6J14, March, 1947.

[2] Underwood, W. J. and Nuber, R. J., "Two-dimensional Wind-tunnel Investigation at High Reynolds Numbers of Two Symmetrical Circular-arc Airfoil Sections with High-lift Devices," NACA RM L6K22, March, 1947.

[3] Morrissette, R. R., and Oborny, L. F., "Theoretical Characteristics of Two-dimensional Supersonic Control Surfaces," NACA RM L8G12, July, 1948.

[4] Boyd, J. W., Katzen, E. D., and Frick, C. W., "Investigation at Supersonic Speed (M=1.53) of the Pressure Distribution over 63° Swept Airfoil of Biconvex Section at Several Angles of Attack," NACA RM A8F22, September, 1948.

[5] Vincenti, W. G., "Comparison Between Theory and Experiment for Wings at Supersonic Speeds," NACA Report 1033, May, 1950.

[6] Ulmann, E. F. and Lord, D. R., "An Investigation of Flow Characteristics at Mach Number 4.04 over 6- and 9-percent-thick Symmetrical Circular-arc Airfoils Having 30-percent-chord Trailing-edge Flaps," NACA RM L51D30, July, 1951.

[7] Chapman, D. R., "Aerodynamic Characteristics of Bodies at Supersonic Speeds, A collection of Three Papers: Base Pressure on Wings and Bodies with Turbulent Boundary Layers," NACA RM A51J25, November, 1951.

[8] Goin, K. L., "Effects of Plan Form, Airfoil Section, and Angle of Attack on the Pressures Along the Base of Blunt-trailing-edge Wings at Mach Numbers of 1.41, 1.62, and 1.96," NACA RM L52D21, September, 1952.

[9] Eggers, A. J. Jr., Syvertson, C. A., and Kraus, S., "A Study of Inviscid Flow About Airfoils at High Supersonic Speeds," NACA Report 1123, January, 1952.

[10] Chapman, D. R., "Airfoil Profiles for Minimum Pressure Drag at Supersonic Velocities – General Analysis with Application to Linearized Supersonic Flow," NACA Report 1063, October, 1952.

[11] Katzen, E. D., Kuehn, D. M., and Hill, W. A. Jr., "Investigation of the Effects of Profile Shape on the Aerodynamic and Structural Characteristics of Thin, Two-dimensional Airfoils at Supersonic Speeds," NACA RM A54B08a, May, 1954.

[12] Dutt, H. N. V. and Sreekanth, A. K., "Design of Supersonic Airfoils by Numerical Optimization," Computer Methods in Applied Mechanics and Engineering, Vol. 19, 1979, pp. 417-427.

[13] Pittman, J. L., "Supersonic Airfoil Optimization," Journal of Aircraft, Vol. 24, No. 12, 1987, pp. 873- 879.

[14] Tai, T. and Moran, M., "Supersonic Low-density Flow Over Airfoils," AIAA paper 89-0530, 1989.

[15] Hu, R., Jameson, A., and Wang, Q., "Adjoint Based Aerodynamic Optimization of Supersonic Biplane Airfoils," AIAA paper 2011-1248, 2011.

[16] Ivey, H. R., Stickle, G. W., and Schuettler, A., "Charts for Determining the Characteristics of Sharp-Nose Airfoils in Two-Dimensional Flow at Supersonic Speeds,". NACA TN 1143,1947.

[17] ANSYS 14.5.7 user guide.